PHOTONICS Research

Broadband nonlinear refraction transients in C-doped GaN based on absorption spectroscopy

FANGYUAN SHI,[1] YUNFEI LV,[1] ZHANPENG CHEN,[1] XINGZHI WU,[1] ZHENGGUO XIAO,[2,5] ZHONGGUO LI,[3] QUANYING WU,[1] YINGLIN SONG,[4,6] AND YU FANG[1,*]

[1]Key Laboratory of Efficient Low-carbon Energy Conversion and Utilization of Jiangsu Provincial Higher Education Institutions, School of Physical Science and Technology, Suzhou University of Science and Technology, Suzhou 215009, China
[2]Department of Physics and Electronic Engineering, Tongren University, Tongren 554300, China
[3]School of Electronic and Information Engineering, Changshu Institute of Technology, Changshu 215500, China
[4]School of Physical Science and Technology, Soochow University, Suzhou 215006, China
[5]e-mail: xiaozhengguo513@163.com
[6]e-mail: ylsong@hit.edu.cn
*Corresponding author: yufang@usts.edu.cn

Received 13 March 2024; revised 31 July 2024; accepted 31 July 2024; posted 2 August 2024 (Doc. ID 523278); published 1 October 2024

Optical nonlinear response and its dynamics of wide-bandgap materials are key to realizing integrated nonlinear photonics and photonic circuit applications. However, those applications are severely limited by the unavailability of both dispersion and dynamics of nonlinear refraction (NLR) via conventional measurements. In this work, the broadband NLR dynamics with extremely high sensitivity ($\lambda/1000$) can be obtained from absorption spectroscopy in GaN:C using the refraction-related interference model. Both the absorption and refraction kinetics are found to be significantly modulated by the C-related defects. Especially, we demonstrate that the refractive index change Δn of GaN:C is negative and can be used to realize all-optical switching applications owing to the large NLR and ultrafast switching time. The NLR under different non-equilibrium carrier distributions originates from the capture of electrons by C_N^+ defect state, while the absorption modulation originates from the excitation of tri-carbon defects. We believe that this work provides a better understanding of the GaN:C nonlinear properties and an effective solution to broadband NLR dynamics of transparent thin films or heterostructure materials. © 2024 Chinese Laser Press

https://doi.org/10.1364/PRJ.523278

1. INTRODUCTION

Materials with optical nonlinearity enable modulation of the intensity, frequency, and phase of optical signals [1–3]. With the in-depth study of optical nonlinear response and the continuous progress of materials technology, it brings new breakthroughs in the field of optics and photonics [4]. Recently, the exceptional optical nonlinearities of wide-bandgap semiconductors have garnered significant interest for the development of nanoscale electronics and on-chip quantum photonics [5–7]. As one of the third-generation wide-bandgap semiconductors, GaN not only has strong adaptability to extreme environments (such as high temperature and high optical power), but also has greater optical nonlinearity and lower application cost than other broadband semiconductors [8]. GaN has a large bandgap of 3.4 eV and exhibits an ultrawide transparency window from the ultraviolet to the mid-infrared. It possesses excellent electrical and optical properties that can satisfy the requirements of high-power electronics and detectors [9–11] and is particularly attractive for applications in optoelectronic platforms [12–16] and compact chip-level nonlinear optics [8,17–20].

All-optical switching (AOS) is regarded as the essential component in photonic processing [21–26]. The applications of AOS in GaN can be realized by two-photon absorption or Kerr refraction with ultrafast switching time [27]. Free-carrier refraction (FCR) is a key mechanism for realizing AOS applications [28–32], and the free-carrier lifetimes can be modulated by the dopants in GaN (such as Fe and C centers). The FCR response is related to numerous factors, including impurities, effective mass, probe polarization, and wavelength. Therefore, it is necessary to effectively extract the nonlinear refraction (NLR) response and its dynamics in different materials. However, traditional pump–probe and newly proposed beam deflection experiments can only study the NLR response at a single wavelength or several discrete wavelengths [33–37]; it consumes much time to carry out multiple experiments to obtain broadband response. On the other hand, the sample needs enough thickness to accumulate the NLR effect through conventional measurements. In addition, time-resolved reflection spectroscopy of opaque samples can be applied to study the broadband NLR dynamics based on supercontinuum [38–40],

but the carrier dynamics process will be mainly affected by surface recombination and carrier diffusion, leading to the NLR dynamics ambiguously.

In this work, we successfully and accurately extract both NLR wavelength dispersion and its dynamics in GaN:C based on transient absorption spectroscopy (TAS) through the interference of the sample. This method can be effectively utilized to measure a micrometer-level sample's NLR (without thickness accumulation) with extremely high sensitivity (10^{-4} order of magnitude for refraction change). Furthermore, via analyzing the NLR dispersion and dynamics, the C doping is found to have strong modulation on the absorption and refraction dynamics of GaN. The research on the ultrafast NLR dynamics shows the potential of GaN:C in the field of AOS. Finally, the modulation mechanisms of carbon doping on the nonlinear absorption (NLA) and NLR in GaN are also analyzed by establishing an excitation and recombination model based on the C defects. Our results prove that it is feasible to extract broadband NLR dynamics from absorption spectroscopy and that this measurement will greatly promote future applications of micro–nano level thin film materials in the field of ultrafast all-optical and photonic devices.

2. EXPERIMENTAL METHOD

The sample C-doped GaN (GaN:C) wafer in this paper is commercially obtained from Suzhou Nanowin Technology Co., Ltd. The GaN film grown by hydride vapor phase epitaxy (HVPE) on sapphire substrate (~400 μm) has a diameter of 2 in. and a thickness of ~4.60 μm. The orientation of the film is [0001], and the density of threading dislocations (TDs) is $\sim 9 \times 10^7\ \mathrm{cm}^{-2}$. The C impurity higher than $10^{19}\ \mathrm{cm}^{-3}$ can compensate the residual donor impurities such as oxygen and silicon, resulting in a semi-insulating (SI) property of GaN:C crystal with resistivity greater than $10^7\ \Omega \cdot \mathrm{cm}$ at 300 K.

In the femtosecond supercontinuum transient absorption measurements, the excitation beam sources used are all tunable laser pulses generated by an optical parametric amplifier (OPA, Light Conversion ORPHEUS) pumped by an ytterbiun-doped fiber laser (Yb:KGW, PHAROS, 1030 nm). The pulse duration (FWHM) and repetition rate are 190 fs and 6 kHz, respectively. One-photon excitation (350–380 nm) is used to generate non-equilibrium carriers with a concentration comparable to that of the C dopant. The probe beam is focused on sapphire media to generate supercontinuum white light (400–800 nm), the entire spectra of the transmitted probe beams were measured using an imaging spectrograph with a Si diode array photodetector, and the broadband carrier dynamics under different time delays can be obtained simultaneously. The spot radii of the pump light and the probe light are 400 μm and 100 μm, respectively. In addition to the ultrafast time-resolved characteristics, more accurate photodynamic information can be obtained by comparing the intensity of white light supercontinuum with different time delays. Optical density (OD) is defined as $-\lg(I_0/I)$, where I_0 and I are the intensities of the incident and transmitted beams, respectively. The OD change (ΔOD) is used to denote the transient absorption response:

$$\Delta \mathrm{OD} = \mathrm{OD}_{\mathrm{pumped}} - \mathrm{OD}_{\mathrm{unpumped}} = \lg\left(\frac{I_{\mathrm{umpumped}}}{I_0}\right) - \lg\left(\frac{I_{\mathrm{pumped}}}{I_0}\right), \tag{1}$$

where I_{unpumped} and I_{pumped} represent the intensity of the supercontinuum white light spectrum transmitted under non-pumped beam and pumped beam, respectively. The ΔOD with high signal-to-noise ratio can be obtained in real time by using a chopper and a lock-in amplifier.

A refraction-related interference model based on NLA is established to obtain nonlinear refraction. The interference arises from two probe beams; the first one is a direct transmission beam through the film (beam 1), and the second one is the reflection beam between the front and rear surfaces of the GaN film (beam 2), as plotted in Fig. 1. The transmittance of the air–GaN interface is $T_1(\lambda) = 4n/(1+n)^2$, where n denotes the real part of the refractive index, which is wavelength dependent and can be expressed as $n(\lambda) = n_0(\lambda) + \Delta n$; $n_0(\lambda)$ and Δn represent the linear refractive index and pump-induced refraction change, respectively. The transmittance $T_s(\lambda)$ of GaN induced by excitation is related to NLA, which can be extracted from the TAS. $R_1(\lambda)$ and $R_2(\lambda)$ are the reflectance of the GaN-sapphire and GaN-air interface, respectively. Therefore, the interference equations for the probe beam at the rear surface of the wafer can be described as

$$I_1(\lambda) = I_0 \times T_1(\lambda) \times T_s(\lambda),$$
$$I_2(\lambda) = I_0 \times T_1(\lambda) \times R_1(\lambda) \times R_2(\lambda) \times T_s^3(\lambda),$$
$$I(\lambda) = I_1(\lambda) + I_2(\lambda) + 2\sqrt{I_1(\lambda) I_2(\lambda)} \cos\left[\frac{2\pi}{\lambda} \times 2\bar{n}(\lambda) d\right], \tag{2}$$

where $I_1(\lambda)$, $I_2(\lambda)$, and $I(\lambda)$ represent the light intensity of the direct transmission light, the reflection light, and the interference light, respectively. $\bar{n}(\lambda)$ is the mean refractive index of the GaN:C film considering the inhomogeneous Δn throughout the film, and d is the thickness of the GaN:C film. All the experiments were carried out at room temperature.

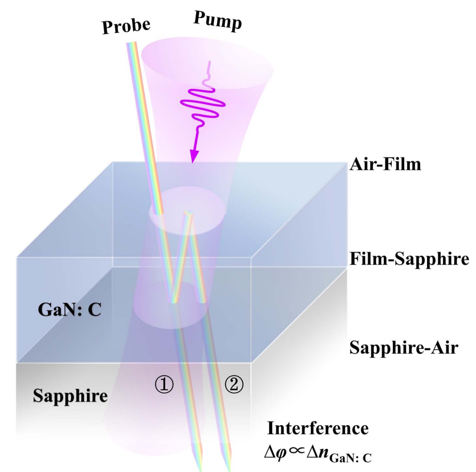

Fig. 1. Schematic diagram of probe light interference.

3. RESULTS AND DISCUSSION

Transient absorption spectroscopy is an effective method to explore the free carrier and defect dynamics in wide-bandgap semiconductors [41,42]. The TAS in GaN:C under different delay times is shown in Fig. 2(a). The oscillation of the TAS originates from the interference effect caused by the light reflection in the GaN:C wafer. The oscillation amplitude in TAS gradually decreases with the delay time and is always accompanied with broadband absorption. The pump fluence-dependent oscillations in TAS at 365 nm, $t_d = 2$ ps, are presented in Fig. 2(b). As the pump fluence increases, in addition to an enhancement of the overall oscillation waveform (absorption response), the amplitudes of the oscillations increase progressively. Due to the strong oscillations in TAS, the absorption spectra need to be averaged and simplified for analyzing the transient spectra. The maximum and minimum values of the adjacent absorption response are averaged ($\Delta\mathrm{mOD}_{\max}/2 + \Delta\mathrm{mOD}_{\min}/2$), and the averaged NLA curves at different delay times are shown in Fig. 2(c). It can be seen that the TAS is an oscillation superimposed on the basis of NLA. Notably, the response is completely different from the free-carrier absorption (monotonically increasing with the probe wavelength) [43,44], indicating that the transient absorption response may come from the defect state-related absorption. To further analyze the oscillations in the spectra, the subtracted spectral oscillation from the averaged NLA at $t_d = 2$ ps, which is defined as pure spectral oscillation, and the pure absorption response (without NLR; see details in Appendix A) are both plotted in Fig. 2(d) for comparison. We surprisingly found that the pure spectral oscillations (amplitude and peak/valley location) are completely different from that induced by pure absorption response. These phenomena imply that, apart from the absorption, the change of refractive index (i.e., nonlinear refraction Δn) in GaN:C must be taken into account. Remarkably, the spectral oscillation may made it completely feasible to extract the NLR based on NLA spectra.

The transient absorption response of GaN:C needs to be initially analyzed before the comprehensive interpretation of nonlinear optical response and effective extraction of NLR. Figure 3 presents the transient absorption dynamics in the GaN:C sample at different excitation fluences [Fig. 3(a)] and pump wavelengths [Fig. 3(b)]. We can observe that the pump fluence does not significantly affect the lifetime, indicating that the defect-related recombination is a major process rather than high-order processes (radiative and Auger recombination). Figure 3(b) shows that the recovery rate of transient absorption

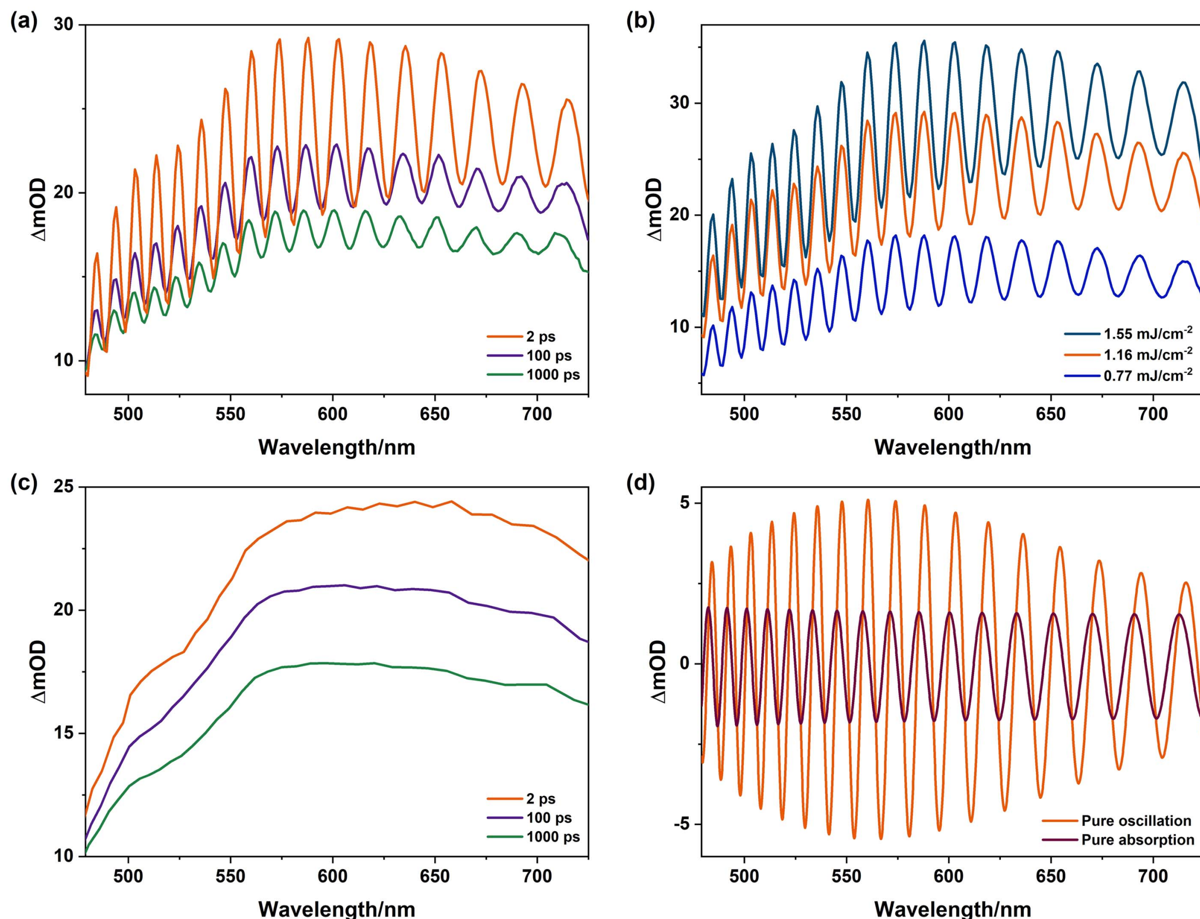

Fig. 2. (a) Transient absorption spectra in GaN:C sample with different delay times. (b) Transient absorption spectra in GaN:C sample with different pump fluences at $t_d = 2$ ps. (c) Transient absorption curves under different delay times in GaN:C sample. (d) The pure oscillation curve extracted by the TAS and the pure absorption spectral oscillation curve at $t_d = 2$ ps in the GaN:C sample. The pump wavelength is 365 nm. In (a), (c), and (d), the pump fluence is 1.16 mJ/cm^2.

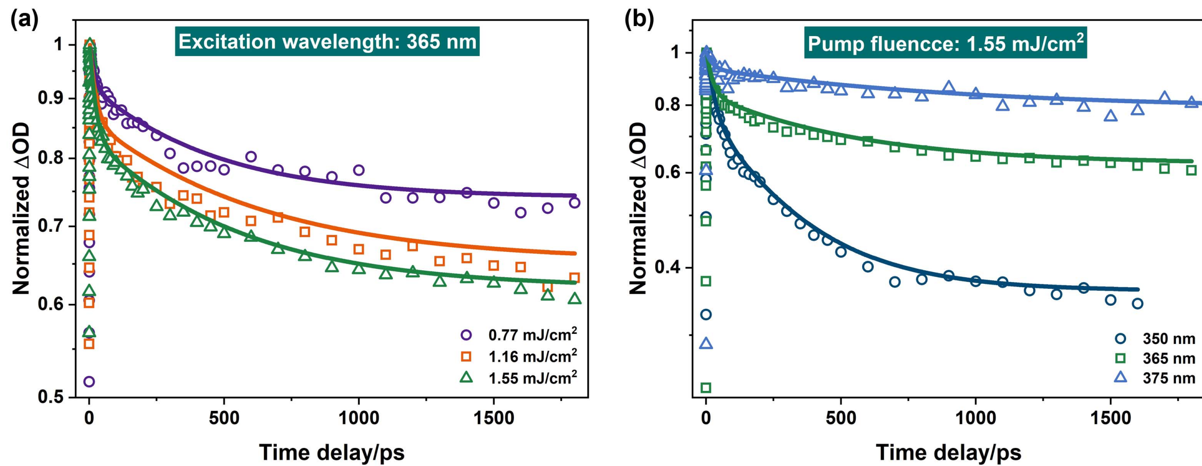

Fig. 3. Semi-logarithmic plot of the transient absorption dynamics in GaN:C sample under (a) various excitation fluences and (b) different pump wavelengths. The probe wavelength is ~600 nm; the solid lines are the theoretical fitting.

becomes slower as the excitation wavelength increases. Furthermore, the semi-logarithmic depiction of the absorption dynamics in Fig. 3 distinctly reveals the presence of both a faster and a slower recovery process. A bi-exponential model with one constant component can be used to well interpret the experimental results. The constant component, faster (slower) lifetimes, and their proportions are listed in Table 1. As the excitation wavelength (E_{photon}) increases (decreases), the concentration of the photo-generated carriers decreases; at the same time, the carrier distribution gradually changes to be more homogeneous (longer depth penetration for the pump beam). The faster lifetime τ_1, which is independent of the excitation and wavelength, should be attributed to the surface recombination, and the effect of surface recombination (lifetime proportion) will decline as the pump wavelength increases. On the other hand, the slower decay component with lifetime τ_2 is supposed to be caused by the trapping of the excited carrier to defect states. As the E_{photon} of the pump decreases, the concentration of the excited defect states decreases, leading to an increase of lifetime τ_2. The constant component (A_0) in bi-exponential fitting indicates the much longer lifetime for carriers trapped on the defect states. Furthermore, the variation trend of the τ_1 (τ_2) and its proportion in recombination with the pump wavelength and fluence at different probe wavelengths is similar to that at 600 nm.

A clear understanding of the spectra and process of transient absorption is conducive to the study of the NLR based on absorption spectroscopy. As the absorption is proved to be modulated by the defect states, the influence of the defect state on the NLR also needs to be discussed. The spectral peak position at different delay times in TAS under the pump wavelength of 365 nm is explored and plotted in Fig. 4(a). As the time delays, the oscillation magnitude of the TAS declines, and the positions of the peaks become blue-shifted. The shifts of the oscillation peaks ($\Delta\lambda$) during the time delay (from 2 to 1600 ps) are presented in Fig. 4(b). The amplitude of the oscillations and the shift of the spectral peaks are potentially associated with both the magnitude and sign of the NLR. Subsequently, the absorption responses under different signs and magnitude of Δn are simulated by using a refraction-related interference model and Eq. (2). As depicted in Fig. 4(c), the peaks of differential ΔmOD will red-shift for $\Delta n > 0$ or blue-shift for $\Delta n < 0$ as the magnitude of the Δn declines during the time delay. Considering the blue-shift of spectral peak with time delay observed in Fig. 4(a), we can infer that the sign of the Δn should be negative. On the other hand, the magnitude of the Δn primarily influences the amplitude of the spectral oscillations, as illustrated in Fig. 4(d). Therefore, the precise values of Δn with respect to the wavelength and time delay can be further ascertained according to the oscillation amplitude's variation.

Figure 5(a) shows the transient absorption spectra ($t_d = 2$ ps) of GaN:C samples excited at 365 nm; the result for GaN:Mg is also presented for comparison [see the inset of Fig. 5(a)]. The interference model presents an excellent fitting to the experimental results, thereby proving the rationality of the interference model. Additionally, the Δn dependence on the probe wavelength at $t_d = 2$ ps, when excited at 350 nm,

Table 1. Fitting Parameters for the Carrier Lifetimes

Pump Wavelength/nm	Pump Power/(mJ/cm^2)	τ_1/ps	τ_2/ps	$A_1/(A_1 + A_2 + A_0)^a$	$A_0/(A_1 + A_2 + A_0)$
350	1.55	25 ± 3	310 ± 20	25.16%	34.86%
365	0.77	20 ± 3	420 ± 30	9.03%	72.95%
365	1.16	20 ± 2	550 ± 50	15.04%	64.35%
365	1.55	20 ± 3	520 ± 30	17.70%	61.20%
375	1.55	21 ± 3	850 ± 70	7.06%	78.30%

[a]The double exponential decay can be expressed as $A(t) = A_1 e^{-t/\tau 1} + A_2 e^{-t/\tau 2} + A_0$.

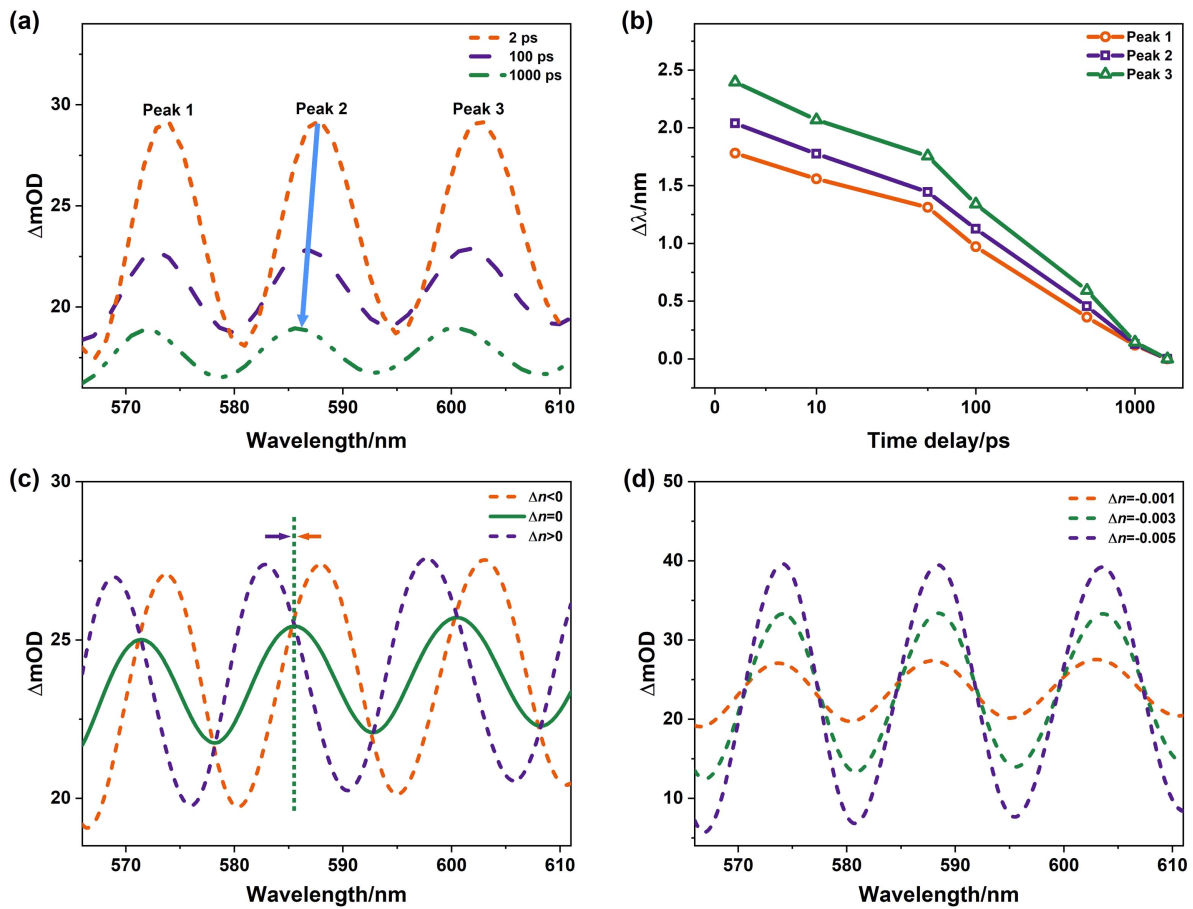

Fig. 4. (a) Transient absorption spectra at 2, 100, and 1000 ps delay time in GaN:C. (b) $\Delta\lambda$ under different delay times. The absorption response of Δn under (c) different signs and (d) different magnitudes is simulated by using the refraction-related interference model. The arrow direction corresponds to the peak offset during the time delays. In both (a) and (b), the pump wavelength is ~365 nm with the pump fluence of ~1.16 mJ/cm^2.

365 nm, and 375 nm, can be extracted and is depicted in Fig. 5(b). Additionally, the Δn dependence on the probe wavelength at $t_d = 2$ ps, when excited at 350 nm, 365 nm, and 375 nm, can be extracted and is depicted in Fig. 5(b). The dispersion of Δn is also different from that of the free carrier; a clear trend (Drude dispersion) in GaN:Mg is shown in the

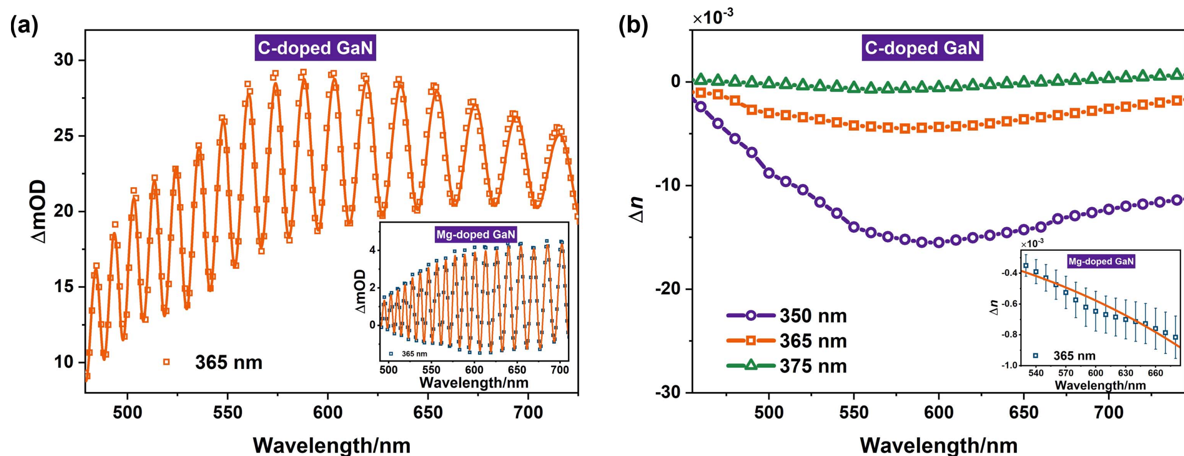

Fig. 5. (a) Transient absorption spectra restored by interference model and Δn ($t_d = 2$ ps) dispersion relation in GaN:C sample (GaN:Mg sample; see inset) with the excitation wavelength of 365 nm. The solid lines are the theoretical fitting. (b) Dispersion curves of the Δn ($t_d = 2$ ps) in GaN:C sample with the excitation wavelengths of 350, 360, and 375 nm. The inset shows a dispersion of Δn ($t_d = 2$ ps) in GaN:Mg at 365 nm. The solid line is the Drude model fitting.

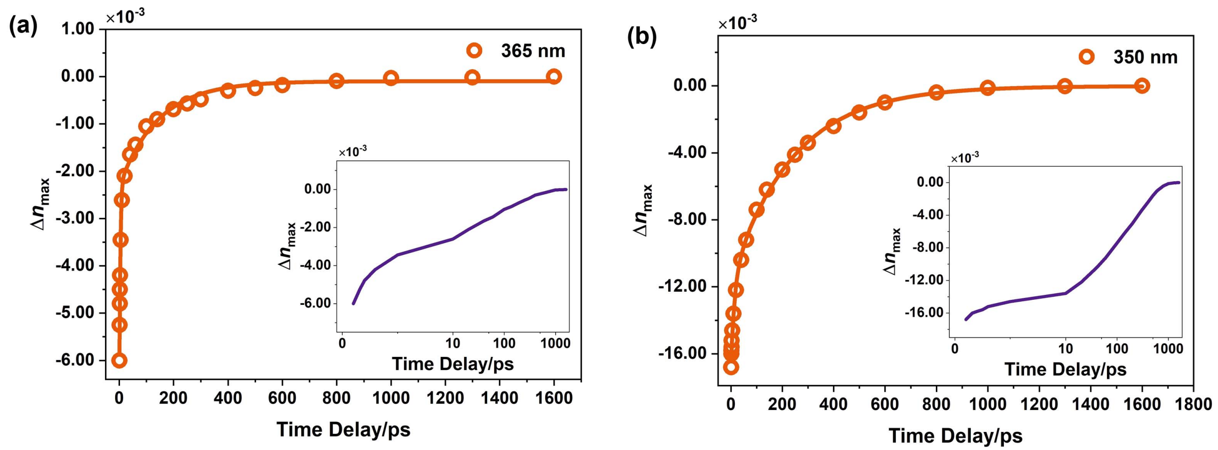

Fig. 6. Maximum Δn dynamics at (a) 365 nm and (b) 350 nm in GaN:C sample with the probe wavelength of ~580 nm. The pump fluence is 1.16 mJ/cm^2. The solid lines are the theoretical fitting, and the inset shows the semi-logarithmic plot under logarithmic coordinates after 10 ps.

inset of Fig. 5(b). Thus, it can be clearly demonstrated that the transient refraction response in the GaN:C sample also arises from the C-related defects. Significantly, one can observe that the sensitivity (the detection limit of the Δn) is on the order of 10^{-4}, corresponding to the wavefront distortion of around $\sim\lambda/1000$, which is about three times higher than that of the conventional Z-scan technique ($\sim\lambda/250$) [45].

The delay time-dependent Δn (i.e., NLR dynamics) probe at ~580 nm in GaN:C at the pump wavelength of 350 nm and 365 nm is presented in Figs. 6(a) and 6(b), respectively. The maximum of Δn value (Δn_{max}) pumped at 365 nm decays to ~50% of the initial value within 10 ps [see the inset of Fig. 6(a)], while it needs nearly 100 ps under 350 nm [see the inset of Fig. 6(b)]. The decay processes can also be fitted with the double exponential decay model, as shown in Appendix B. The $\tau_{on/off}$, defined as switching time (Δn_{max} decays to ~50% of the maximum), can be obtained at different excitation wavelengths. The $\tau_{on/off}$ is gradually reduced with the increase of excitation wavelength, and the detailed results are summarized in Table 2. The Δn_{max} and switching of GaN:C are at least one order of magnitude larger and faster than that of GaN:Mg under the same condition, respectively. As a result, GaN:C could serve as a potential candidate for integrated AOS based on the C-related defect NLR. Compared to the slightly larger NLR under excitation of 360 nm, a much shorter $\tau_{on/off}$ (~18% of 360 nm) under 365 nm enables faster modulation of the optical signal. Although the fastest response time can be achieved at 375 nm, the much lower NLR is not suitable for the AOS.

Table 2. Fitting Parameters for $\tau_{on/off}$ of GaN:C and GaN:Mg Samples

Sample	Pump Wavelength/nm	$\Delta n_{max}/10^{-3}$	$\tau_{on/off}$/ps
GaN:C	350	−16.80	86 ± 6
GaN:C	360	−11.26	34 ± 3
GaN:C	365	−6.00	6 ± 0.2
GaN:C	375	−1.00	4 ± 0.2
GaN:Mg	365	−0.79	57 ± 5

Our results demonstrate that the value, sign, and dispersion relation of Δn can be all obtained based on the TAS via interference model. Moreover, the dynamics of Δn combined with TAS can help us to further analyze the defect-related carrier trapping mechanisms in GaN:C. The evidence suggests that the carbon in GaN mainly exists in the form of isolated carbon, dicarbon, and tri-carbon complexes at high doping [46–49]. When the carbon doping concentration [C] exceeds 10^{18} cm^{-3}, the tri-carbon becomes the dominant defect [47], and the concentration of C_N (~10^{18} cm^{-3}) and tri-carbon (~10^{19} cm^{-3}) defects is at least one order of magnitude greater than that of other C-related defects (<10^{17} cm^{-3}) especially for [C] > 10^{19} cm^{-3} [48,49]. Therefore, in our GaN:C, the C_N and tri-carbon defects are considered to be major defects. A defect state capture level model based on the characteristics of these two defects can be established, which is plotted in Fig. 7(a). The defect charge conversions during excitation and trapping processes can interpret the modulation mechanisms of the transient absorption and refraction dynamics. Under one-photon excitation (1PE), the electrons in the valence band (VB) absorb the energy of the photon and then transfer to the conduction band (CB), producing non-equilibrium carrier concentrations greater than 10^{18} cm^{-3}. The electrons in the tri-carbon defect (0/+ transition level) can also transfer to the CB by 1PE. Because of the compensation mechanism, the tri-carbon defects are 0 charge state before excitation. According to the first-principles calculations, the +1 charge state belonging to the negative-U center is not stable in equilibrium [48], but it can be generated by illumination [50]. At present, the position of the (0/+2) is determined at about 2.15 eV above the Fermi energy level. Based on the relationship between formation energy and Fermi level as well as the negative U behavior for the +1 charge state, the position of the (0/+1) transition level is about 1.5–2.5 eV below the minimum of the CB and ~1–2 eV above the maximum of the VB. These energies are very close to the broadband absorption feature in TAS experiment considering the lattice relaxation, and therefore the transient absorption modulation is supposed to be related to the tri-carbon defect. As a result, the electrons in the

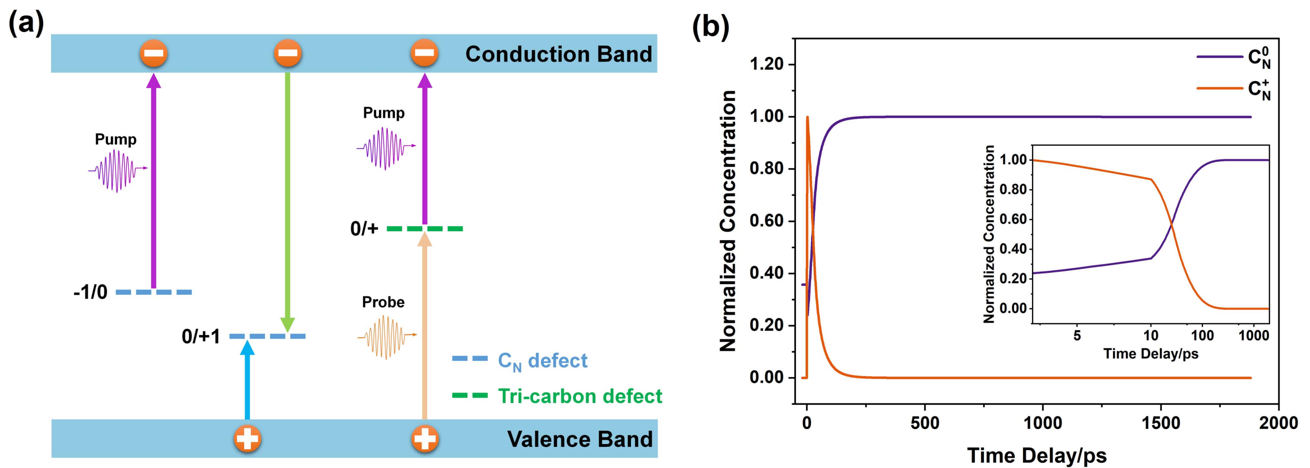

Fig. 7. (a) Excitation and capture processes for the transition of different charge states of C_N and tri-carbon defects. (b) Transiens C_N concentration simulated by the rate equation.

VB may transfer to the tri-carbon defect (+ charge state) by absorbing probe light, causing the absorption response in TAS, which also explains the non-zero absorption after a rapid decay, as shown in Fig. 3. The C_N defect, on the other hand, can only absorb the photons in the near-infrared region, and thus no absorption response will be observed during the visible detection window.

There is a direct relationship between the n and the real part of the dielectric function $\varepsilon(\omega): n \approx \mathrm{Re}[\varepsilon(\omega)^{1/2}]$ for transparent materials (see Appendix C for details). The $\varepsilon(\omega)$ is related to many factors, such as the electron concentration in different states (CB, defect state, and VB), the location of the defect in the bandgap, and the probe wavelength [51]. Based on the previous analysis, the ϕ_1 factor associated with free-carrier refraction can be initially disregarded. Moreover, considering that the broadband absorption response is modulated by the excitation of the tri-carbon defect, the photon energy of the probe (ω) and the energy difference between the VB and the tri-carbon defect (ω_{tr}) are roughly equal, ranging from approximately 1.5 to 2.5 eV, and the width of the transition ($1/\tau_{12}$) is greater than 1 eV. Under these conditions, the sign conversion of $\mathrm{Re}(\phi_2)$ occurs across the probe wavelength spectrum and the $\mathrm{Re}(\phi_2)$ is calculated to be approximately zero simultaneously [52]. Consequently, the contribution of the tri-carbon defect to the NLR can be negligible. Thus, we further focus on the modulation of C_N on the refraction dynamics. Before optical excitation, the –1 charge state is dominant for the C_N defect [53,54], so we discuss the source of C_N^0 and C_N^+, respectively. The C_N^0 states come from (1) the charge transfer by the pump light ($C_N^- \rightarrow C_N^0 + e^-$), (2) the hole capture process through C_N^- ($C_N^- + h^+ \rightarrow C_N^0$), and (3) the electron capture process through C_N^+ ($C_N^+ + e^- \rightarrow C_N^0$). However, the C_N^+ states can be generated via a sole way: the hole capture process via C_N^0 ($C_N^0 + h^+ \rightarrow C_N^+$). The rate equation (see Appendix D for details) can be established based on the above analysis, which can simulate the concentration of C_N-related defect states. The simulated dynamics shows that the dynamic process of C_N^+ defect states agrees well with the experimental NLR dynamics, as shown in Fig. 7(b). Therefore, the modulation of refraction dynamics is probably attributed to the C_N^+ state. Moreover, the C_N^+ state will quickly capture the electrons in the CB after excitation [55], corresponding to the fast recovery of the NLR dynamics. Note that the recovery time of refraction at 350 nm excitation is slower than 365 nm. This can be explained by the increased concentration of the C_N^+ state induced by pump light ($C_N^0 \rightarrow C_N^+ + e^-$), and therefore the decay of the C_N^+ state slows down through the hole trapping of C_N^0. For the shallow trap of the C_N^+, the ω_{tr} (~0.4 eV) is significantly smaller than the probe energy ω [56,57]. This results in a negative sign for the $\mathrm{Re}(\phi_2)$, which aligns with the extracted Δn. Notably, the sign and dynamics of the Δn induced by the C_N^+ defect state are in harmony with the predictions derived from the dielectric and rate equations. Our results not only distinguish the effects of different carbon defects (isolated C_N and tri-carbon) on carrier capture dynamics from the perspective of both absorption and refraction response, but also elaborate on their contributions to NLA and NLR, providing a deeper and clearer understanding of the dynamics of C-related defects in GaN.

4. CONCLUSION

To summarize, broadband NLR and its dynamics in C-doped GaN were systematically studied based on absorption spectroscopy. The TAS presents an oscillation superimposed on the basis of NLA. The transient absorption dynamics shows that the absorption kinetics primarily depends on the surface recombination and carbon-related recombination. Using a refraction-related interference model based on NLA, we demonstrate that the blue-shift of spectral peaks is mainly caused by a negative Δn, and the wavelength dependence of Δn is different from that of free carrier. Remarkably, the sensitivity of Δn using the interference model is up to $\sim 10^{-4}$, corresponding to the wavefront distortion of $\sim\lambda/1000$. The refraction dynamics indicates that the NLR of GaN:C has an ultrafast switching time (<10 ps) and the Δn_{max} is at least one order of magnitude larger than that of GaN:Mg. Finally, the energy level model based on C-related defect was established. The modulation

of refraction dynamics comes from the capture of electrons by the C_N^+ state, while the NLA modulation originates from the transition of tri-carbon defect charge state. The extremely high sensitivity method for the NLR measurements based on TAS can be applied to the broadband nonlinear optical measurements for thin film, composite film, and other two-dimensional materials in micro–nano level, promoting future applications in the field of ultrafast all-optical and integrated photonic devices.

APPENDIX A: SIMULATED ABSORPTION RESPONSE

The change of interference intensity depends on the phase difference, and it can be expressed by $k \times 2n(\lambda)d$, where $k = 2\pi/\lambda$. The refraction-related interference model is used to simulate the absorption response $\Delta\mathrm{mOD} = 10^{-3}\Delta\mathrm{OD}$ without/with pump excitation when $\Delta n = 0$, and the ΔmOD induced by pure NLA response with transmittance $T_s = 0.96$ is calculated, as shown in Fig. 8. We have shifted downward the curve in Fig. 8(c) for better comparison, which is plotted in Fig. 2(d).

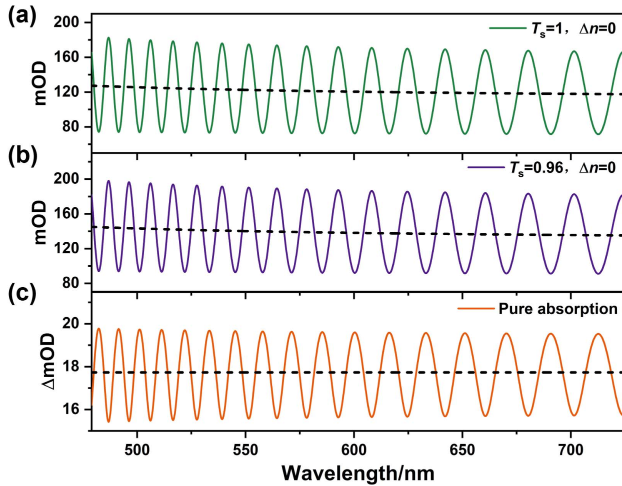

Fig. 8. Absorption response (a) without pump excitation and (b) with pump excitation simulated by interference model. (c) ΔmOD obtained by subtracting (a) from (b). The dashed lines represent the absorption responses without light interference.

APPENDIX B: TRANSIENT REFRACTION DYNAMICS UNDER DIFFERENT EXCITATION WAVELENGTH

Transient refraction dynamics of GaN:C samples at other excitation wavelengths and also extracted refraction dynamics of GaN:Mg at 365 nm are shown in Fig. 9.

APPENDIX C: DIELECTRIC FUNCTION MODEL

The dielectric function $\varepsilon(\omega)$ of semiconductors is given by

$$\varepsilon(\omega) = 1 + \frac{e^2}{m\varepsilon_0}(N_0 - N_{\mathrm{CB}} - N_{\mathrm{tr}}) f_{12} \frac{1}{\omega_{12}^2 - \omega^2 - i\omega/\tau_{12}} + \frac{e^2}{\varepsilon_0} \times (\phi_1 + \phi_2) + \chi_{\mathrm{eff}}^3 E_p^2,$$
$$\phi_1 = -\frac{N_{\mathrm{CB}} f_{\mathrm{CB}}}{m^*} \frac{1}{\omega^2 + i\omega/\tau_{e-p}},$$
$$\phi_2 = \frac{N_{\mathrm{tr}} f_{\mathrm{tr}}}{m} \frac{1}{\omega_{\mathrm{tr}}^2 - \omega^2 - i\omega/\tau_{\mathrm{tr}}}, \tag{C1}$$

where m (m^*) is the electron mass (effective mass), ε_0 is the vacuum permittivity, and N_0, N_{CB}, and N_{tr} are the density of valence band electrons, conduction band electrons, and trapped electrons (bandgap), respectively. f_{CB} is the oscillator strength standing for the transitions occurring in the CB, and $1/\tau_{\mathrm{e-p}}$ simulates the electron–phonon collisions in the CB. ω is the probe energy. ω_{tr} is the energy difference between the VB and the first excited state of the induced defect; $1/\tau_{\mathrm{tr}}$ is the width of this transition. f_{tr} is its corresponding oscillator strength. $1/\tau_{12}$ is the width of the transition. χ_{eff}^3 is an effective third-order nonlinear susceptibility, and E_p is the electric field associated with the pump laser pulse. ϕ_1 is always negative, which is proportional to the density of electrons that have been excited by the pump pulse in the CB. The last term stands for the trapping of the electrons subsequent to a defect formation.

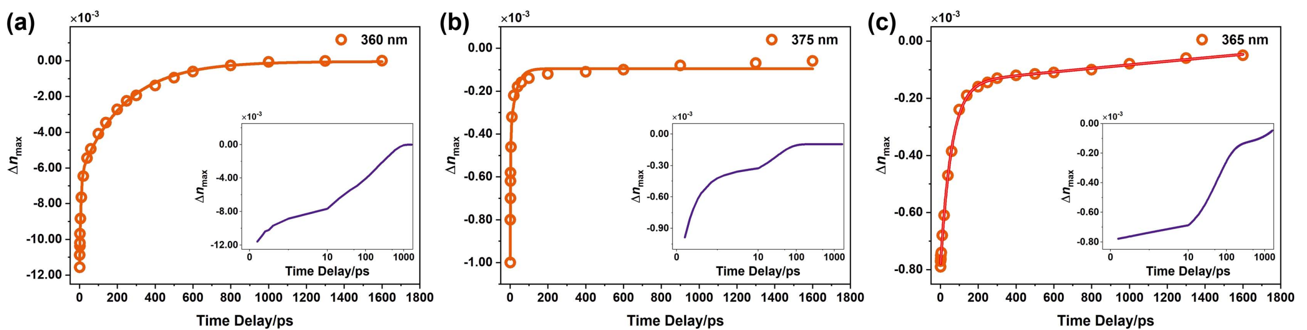

Fig. 9. Maximum Δn dynamics at (a) 360 nm and (b) 375 nm in GaN:C sample. (c) Maximum Δn dynamics at 365 nm in GaN:Mg sample. Probe wavelength is ~580 nm, and the pump fluence is 1.16 mJ/cm^2. The solid lines are the theoretical fitting, and the inset shows the semi-logarithmic plot under logarithmic coordinates after 10 ps.

APPENDIX D: RATE EQUATIONS BASED ON CARRIER TRAPPING

The rate equations according to the model are described as

$$\begin{aligned}
\frac{\mathrm{d}n}{\mathrm{d}t}&=\frac{\alpha_0 I}{\hbar\omega}+\frac{\sigma_0 I N_-}{\hbar\omega}+\frac{\sigma_1 I N_0}{\hbar\omega}-C_{\mathrm{n1}}\Delta n N_0-C_{\mathrm{n2}}\Delta n N_+-\frac{\Delta n}{\tau},\\
\frac{\mathrm{d}p}{\mathrm{d}t}&=\frac{\alpha_0 I}{\hbar\omega}-C_{\mathrm{p1}}\Delta p N_- - C_{\mathrm{p2}}\Delta p N_0-\frac{\Delta p}{\tau},\\
\frac{\mathrm{d}N_0}{\mathrm{d}t}&=\frac{\sigma_0 I N_-}{\hbar\omega}-\frac{\sigma_1 I N_0}{\hbar\omega}+C_{\mathrm{p1}}N_-\Delta p-C_{\mathrm{p2}}N_+\Delta p\\
&\quad -C_{\mathrm{n1}}N_0\Delta n+C_{\mathrm{n2}}N_+\Delta n,\\
\frac{\mathrm{d}N_+}{\mathrm{d}t}&=\frac{\sigma_1 I N_0}{\hbar\omega}+C_{\mathrm{p2}}N_0\Delta p-C_{\mathrm{n2}}N_+\Delta n,\\
N_-&=N_t-N_0-N_+,
\end{aligned} \tag{D1}$$

where Δn and Δp are the non-equilibrium carrier concentration of electrons and holes, α_0 is one-photon absorption coefficient, and I is the light intensity of the pump beam. σ_0 and σ_1 represent the absorption cross section where the outer electrons of C_N^- and C_N^0 are ionized into the CB by the pump light, respectively. N_t represents the concentrations of the total receptor (defect), and N_0, N_+, and N_- are the concentrations of C_N^0, C_N^+, and C_N^-, respectively. C_{n1} and C_{n2} are the electron capture coefficients of C_N^- and C_N^+, and C_{p1} and C_{p2} are the hole trapping coefficients of C_N^- and C_N^0. The relevant parameters used for the simulation of defect dynamics were extracted from Refs. [55] and [56].

Funding. National Natural Science Foundation of China (11704273, 12374300); Natural Science Foundation of Jiangsu Province (BK20221384); Jiangsu Key Disciplines of the Fourteenth Five-Year Plan (2021135); Postgraduate Research & Practice Innovation Program of Jiangsu Province (KYCX22_3267); Science and Technology Innovation Team of Guizhou Education Department ([2023]094); Science and Technology Foundation of Guizhou Province (ZK [2023]049).

Disclosures. The authors declare no conflicts of interest.

Data Availability. Data underlying the results presented in this paper are not publicly available at this time but may be obtained from the authors upon reasonable request.

REFERENCES

1. H. Ma, D. Li, N. Wu, *et al.*, "Nonlinear all-optical modulator based on non-Hermitian PT symmetry," Photonics Res. **10**, 980–988 (2022).
2. Y. Hu, Z. Yang, T. Zhang, *et al.*, "Nonlinear optical response and ultrafast all-optical modulation of Nb_4C_3," Opt. Express **31**, 19722–19732 (2023).
3. Q. Yi, Y. Feng, D. Liu, *et al.*, "Broadband nanosecond pulse generation modulated by zirconium triselenide nanoflakes," Opt. Mater. Express **13**, 997–1006 (2023).
4. W. Xie, C. Xiang, L. Chang, *et al.*, "Silicon-integrated nonlinear III-V photonics," Photonics Res. **10**, 535–541 (2022).
5. D. J. Wilson, K. Schneider, S. Hönl, *et al.*, "Integrated gallium phosphide nonlinear photonics," Nat. Photonics **14**, 57–62 (2020).
6. D. M. Lukin, C. Dory, M. A. Guidry, *et al.*, "4H-silicon-carbide-on-insulator for integrated quantum and nonlinear photonics," Nat. Photonics **14**, 330–334 (2020).
7. F. Baboux, G. Moody, and S. Ducci, "Nonlinear integrated quantum photonics with AlGaAs," Optica **10**, 917–931 (2023).
8. Y. Zheng, C. Sun, B. Xiong, *et al.*, "Integrated gallium nitride nonlinear photonics," Laser Photonics Rev. **16**, 2100071 (2022).
9. S. Zhou, H. Xu, B. Tang, *et al.*, "High-power and reliable GaN-based vertical light-emitting diodes on 4-inch silicon substrate," Opt. Express **27**, A1506–A1516 (2019).
10. Z. Xu, Z. Luo, X. Lin, *et al.*, "15.26 Gb/s Si-substrate GaN high-speed visible light photodetector with super-lattice structure," Opt. Express **31**, 33064–33076 (2023).
11. T. Cheng, T. Fei, W. Zhang, *et al.*, "Ellipsometric and first-principles study on temperature-dependent UV–Vis dielectric functions of GaN," Appl. Opt. **60**, 6869–6877 (2021).
12. N. Aggarwal and G. Gupta, "Enlightening gallium nitride-based UV photodetectors," J. Mater. Chem. C **8**, 12348–12354 (2020).
13. Y. Jiang, A. He, R. Zhao, *et al.*, "Coexistence of photoelectric conversion and storage in van der Waals heterojunctions," Phys. Rev. Lett. **127**, 217401 (2021).
14. Y. Yang, W. Wang, Y. Zheng, *et al.*, "Defect effect on the performance of nonpolar GaN-based ultraviolet photodetectors," Appl. Phys. Lett. **118**, 053501 (2021).
15. W. Wang, C. Chu, J. Che, *et al.*, "Is a thin p-GaN layer possible for making high-efficiency AlGaN-based deep-ultraviolet light-emitting diodes?" Opt. Express **29**, 29651–29660 (2021).
16. B. Wang, K. Fu, J. Fu, *et al.*, "Miniature GaN optoelectronic temperature sensor," Opt. Lett. **48**, 4209–4212 (2023).
17. E. Stassen, M. Pu, E. Semenova, *et al.*, "High-confinement gallium nitride-on-sapphire waveguides for integrated nonlinear photonics," Opt. Lett. **44**, 1064–1067 (2019).
18. K. Li, W. Fu, and H. Choi, "Chip-scale GaN integration," Prog. Quantum Electron. **70**, 100247 (2020).
19. X. Li, Y. Wang, K. Hane, *et al.*, "GaN-based integrated photonics chip with suspended LED and waveguide," Opt. Commun. **415**, 43–47 (2018).
20. F. Shi, H. Zhang, C. Jiang, *et al.*, "Collinear optical links based on a GaN-integrated chip for fiber-optic acoustic detection," Opt. Lett. **49**, 169–172 (2024).
21. Y. Wang, S. He, X. Gao, *et al.*, "Enhanced optical nonlinearity in a silicon–organic hybrid slot waveguide for all-optical signal processing," Photonics Res. **10**, 50–58 (2022).
22. G. Grinblat, M. P. Nielsen, P. Dichtl, *et al.*, "Ultrafast sub–30-fs all-optical switching based on gallium phosphide," Sci. Adv. **5**, eaaw3262 (2019).
23. S. Hua and W. Zhang, "Multiphoton absorption and dispersive nonlinear refraction of ZnO in VIS-NIR bands," Opt. Laser Technol. **145**, 107478 (2022).
24. S. Hua and W. Zhang, "Anisotropy of 2PA, 3PA, and Kerr effect in nonpolar ZnO," Opt. Lett. **46**, 4065–4068 (2021).
25. S. Hua and W. Zhang, "Three-photon-induced free-carrier absorption in Ga-doped ZnO," Opt. Lett. **47**, 273–276 (2022).
26. L. Li, X. Guo, P. Ding, *et al.*, "Ultrafast all-optical switching in the visible spectrum with 6H silicon carbide," ACS Photonics **8**, 2940–2946 (2021).
27. F. Shi, Z. Li, X. Wu, *et al.*, "Broadband optical nonlinearity and all-optical switching features in low-defect GaN," Opt. Express **31**, 32263–32272 (2023).
28. M. A. A. Bakar, S. K. Alsaee, J. B. H. Ooi, *et al.*, "GaN film optical nonlinearity: wavelength dependent refractive index for all-optical switching application," Opt. Laser Technol. **166**, 109642 (2023).
29. Y. Hu, J. You, M. Tong, *et al.*, "Pump-color selective control of ultrafast all-optical switching dynamics in metaphotonic devices," Adv. Sci. **7**, 2000799 (2020).
30. Z. Chai, X. Hu, F. Wang, *et al.*, "Ultrafast all-optical switching," Adv. Opt. Mater. **5**, 1600665 (2017).
31. M. R. Shcherbakov, P. P. Vabishchevich, A. S. Shorokhov, *et al.*, "Ultrafast all-optical switching with magnetic resonances in nonlinear dielectric nanostructures," Nano Lett. **15**, 6985–6990 (2015).
32. B.-J. Huang, C.-T. Tsai, Y.-H. Lin, *et al.*, "SiGeC waveguide for all-optical data switching," ACS Photonics **5**, 2251–2260 (2018).

33. X. Jiang, S. Liu, W. Liang, *et al.*, "Broadband nonlinear photonics in few-layer MXene $Ti_3C_2T_x$ (T = F, O, or OH)," Laser Photonics Rev. **12**, 1700229 (2018).
34. P. Zhao, M. Reichert, D. J. Hagan, *et al.*, "Dispersion of nondegenerate nonlinear refraction in semiconductors," Opt. Express **24**, 24907–24920 (2016).
35. M. R. Ferdinandus, H. Hu, M. Reichert, *et al.*, "Beam deflection measurement of time and polarization resolved ultrafast nonlinear refraction," Opt. Lett. **38**, 3518–3521 (2013).
36. S. Benis, N. Munera, S. Faryadras, *et al.*, "Extremely large nondegenerate nonlinear index and phase shift in epsilon-near-zero materials," Opt. Mater. Express **12**, 3856–3871 (2022).
37. M. Reichert, P. Zhao, J. M. Reed, *et al.*, "Beam deflection measurement of bound-electronic and rotational nonlinear refraction in molecular gases," Opt. Express **23**, 22224–22237 (2015).
38. J. Xue, R. Wang, X. Chen, *et al.*, "Reconfiguring the band-edge states of photovoltaic perovskites by conjugated organic cations," Science **371**, 636–640 (2021).
39. J. Tong, Z. Song, D. H. Kim, *et al.*, "Carrier lifetimes of >1 μs in Sn-Pb perovskites enable efficient all-perovskite tandem solar cells," Science **364**, 475–479 (2019).
40. Y. Zhai, K. Wang, F. Zhang, *et al.*, "Individual electron and hole mobilities in lead-halide perovskites revealed by noncontact methods," ACS Energy Lett. **5**, 47–55 (2019).
41. Y. Mao, H. Wang, I. Kislyakov, *et al.*, "Nonlinear optical properties and ultrafast carrier dynamics of ultrathin $ReSe_2$," Opt. Lett. **48**, 6259–6262 (2023).
42. C. Chen, N. Dong, J. Huang, *et al.*, "Microscopic optical nonlinearities and transient carrier dynamics in indium selenide nanosheet," Opt. Express **30**, 17967–17979 (2022).
43. E. Kioupakis, P. Rinke, A. Schleife, *et al.*, "Free-carrier absorption in nitrides from first principles," Phys. Rev. B **81**, 241201 (2010).
44. P. Ščajev, K. Jarašiūnas, Ü. Özgür, *et al.*, "Anisotropy of free-carrier absorption and diffusivity in m-plane GaN," Appl. Phys. Lett. **100**, 022112 (2012).
45. M. Sheik-Bahae, A. A. Said, and E. W. Van Stryland, "High-sensitivity, single-beam n_2 measurements," Opt. Lett. **14**, 955–957 (1989).
46. I. Gamov, E. Richter, M. Weyers, *et al.*, "Carbon doping of GaN: proof of the formation of electrically active tri-carbon defects," J. Appl. Phys. **127**, 205701 (2020).
47. K. Irmscher, I. Gamov, E. Nowak, *et al.*, "Tri-carbon defects in carbon doped GaN," Appl. Phys. Lett. **113**, 262101 (2018).
48. J. L. Lyons, E. R. Glaser, M. E. Zvanut, *et al.*, "Carbon complexes in highly C-doped GaN," Phys. Rev. B **104**, 075201 (2021).
49. Z. Shen, X. Yang, S. Wu, *et al.*, "Mechanism for self-compensation in heavily carbon doped GaN," AIP Adv. **13**, 035026 (2023).
50. J. Neugebauer and C. G. Van de Walle, "Hydrogen in GaN: novel aspects of a common impurity," Phys. Rev. Lett. **75**, 4452–4455 (1995).
51. P. Martin, S. Guizard, P. Daguzan, *et al.*, "Subpicosecond study of carrier trapping dynamics in wide-band-gap crystals," Phys. Rev. B **55**, 5799–5810 (1997).
52. L. Guo, X. Xu, and J. R. Salvador, "Ultrafast carriers dynamics in filled-skutterudites," Appl. Phys. Lett. **106**, 231902 (2015).
53. M. Matsubara and E. Bellotti, "A first-principles study of carbon-related energy levels in GaN. I. Complexes formed by substitutional/interstitial carbons and gallium/nitrogen vacancies," J. Appl. Phys. **121**, 195701 (2017).
54. S. Wu, X. Yang, H. Zhang, *et al.*, "Unambiguous identification of carbon location on the N site in semi-insulating GaN," Phys. Rev. Lett. **121**, 145505 (2018).
55. Y. Fang, X. Wu, J. Yang, *et al.*, "Carrier trapping and recombination at carbon defects in bulk GaN crystals grown by HVPE," Appl. Phys. Lett. **118**, 112105 (2021).
56. M. Reshchikov, M. Vorobiov, D. Demchenko, *et al.*, "Two charge states of the C N acceptor in GaN: Evidence from photoluminescence," Phys. Rev. B **98**, 125207 (2018).
57. J. Lyons, A. Janotti, and C. Van de Walle, "Effects of carbon on the electrical and optical properties of InN, GaN, and AlN," Phys. Rev. B **89**, 035204 (2014).